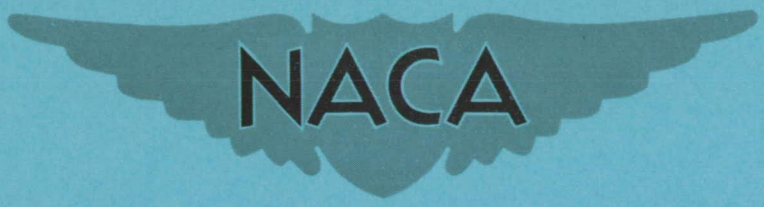

RESEARCH MEMORANDUM

INVESTIGATION OF THE FATIGUE STRENGTH OF FULL-SCALE AIRPLANE WING STRUCTURES

By Dwight O. Fearnow

Langley Aeronautical Laboratory
Langley Field, Va.

NATIONAL ADVISORY COMMITTEE
FOR AERONAUTICS

WASHINGTON

July 13, 1951

NATIONAL ADVISORY COMMITTEE FOR AERONAUTICS

RESEARCH MEMORANDUM

INVESTIGATION OF THE FATIGUE STRENGTH OF FULL-SCALE AIRPLANE WING STRUCTURES

By Dwight O. Fearnow

SUMMARY

Results are presented of a fatigue-strength investigation of a typical full-scale airplane wing structure. The tests were conducted by the resonant-frequency method, wherein concentrated masses were attached to the wing to reproduce flight stresses corresponding to load-factor values of 1 ± 0.625g over approximately 45 percent of the span. The results presented include the data obtained on the first two specimens of a more complete program.

Although the results cover 11 fatigue cracks, the amount of data is as yet insufficient to warrant definite conclusions. The data indicate a surprisingly small amount of spread in fatigue life even though all fatigue cracks did not originate at the same points. Computed effective stress-concentration factors for similar riveted joints varied from 2.55 to 3.15, whereas the one value computed for the corner of an inspection hole cut-out was 4.20. Neither the natural frequency nor the damping of the two test specimens appeared to be affected by fatigue damage until after a fatigue crack had originated; thus, indications are that the use of these parameters may not be adequate as a measure of the damage caused by fatigue in an airplane wing structure. The rate of fatigue crack growth was quite small until the crack had included approximately 7.5 percent of the tension material. Beyond this value, the rate of crack growth increased very rapidly.

INTRODUCTION

Recent trends in airplane design, construction, and use have placed increasing emphasis upon the problem of fatigue in airplane structures. Unfortunately, an exact theoretical method of computing fatigue life is not available. Moreover, most fatigue tests to date have been conducted on small polished specimens under closely controlled

laboratory conditions and, although such basic tests are essential to the solution of the problem, they do not reproduce all the practical problems of a complex wing structure.

When it became apparent that war surplus airplanes could be made available for research, the NACA Special Committee on Surplus Aircraft Research endorsed the proposal that an investigation of the fatigue strength of airplane structures be carried out through the testing of surplus aircraft. Since the scatter in most fatigue data is so large, it is necessary in any fatigue investigation to test a large number of specimens under identical test conditions. A statistical analysis of the data can then be made. The original proposal for fatigue research on full-scale airplanes covered the testing of 600 airplanes of 15 different types. As an initial phase of the program, it was recommended that the NACA carry out an investigation on one type of transport airplane. Accordingly 23 C-46 airplanes were secured from the War Assets Administration.

The important objective of the program is to determine, if possible, how the results of laboratory tests on small specimens can be applied to full-scale wing structures. This objective could possibly be accomplished by comparing the results of the present tests with results from other investigations which have been made in fatigue laboratories on mock-ups of such stress raisers as riveted joints and inspection cut-outs. Other objectives are (1) the determination of the spread in fatigue life, (2) the reduction in static strength after fatigue failure, (3) the effect of fatigue damage on such parameters as natural frequency and damping characteristics, and (4) the loss in fatigue life associated with the number of hours a transport-type airplane has flown.

The present report covers the testing technique and the results available from the first two airplane wing structures. The tests reported were of the constant-level type in which the wing was subjected to stresses corresponding to an arbitrary load factor increment of $1 \pm 0.625g$, or approximately 22 ± 14 percent of estimated design ultimate load factor.

APPARATUS

Description of wing structure.- The two C-46D wings used in the present investigation had previously been subjected to approximately 600 hours of flight service and several years storage in an open depot. The geometric characteristics of the wing, together with various other pertinent parameters of the airplane, are given in table 1.

The wings are of all-metal, riveted, stressed-skin construction. The main beams or spars consisted of spar caps and shear webs. The spar caps were relatively heavy T-shaped extrusions, whereas the shear webs were sheet material reinforced by extruded angles. All material in the spars was 24S-T aluminum alloy. The skin was supported not only by the spars but also by hat-section stiffeners which were made from rolled sheet-stock and laid parallel to the 70-percent-chord spar. The skin and stiffener material was all alclad 24S-T.

The wings were constructed in three parts; two outer panels, and a center section. The center section was continuous through the fuselage and supported the two engine nacelles and the landing gear. The ribs in the center section were of the truss type made of 24S-T sheet-metal formings.

The outer panels were set at a dihedral angle of 7° and were attached to the center section by extruded angles and high-strength bolts. The ribs in the outer panels were of the conventional web type made of 24S-T sheet material. The outer panels were of two-spar construction with one spar at the 30-percent-chord position and the other at the 70-percent-chord position. The spar at the 70-percent-chord position was straight and perpendicular to the center line of the airplane. The center section had, in addition to the 30- and 70-percent-chord position spars, an auxiliary spar located at about the 20-percent-chord position. All skin joints were riveted and were either butt or lap joints.

Preparation of wing for testing.- To prepare the airplanes for the fatigue tests, the following modifications were made. The fuselage forward of and behind the wing was cut off beyond the wing fuselage attachment points. The outer wing panels were cut off at the wing station 405 inches from the center line of the wing-fuselage combination so that the total span of the wing was reduced from 1296 inches to 810 inches. The shear material of the two spars in both the left and right outer panels was substantially increased from wing stations 305 to 405 to accommodate concentrated masses, or weight boxes, which were used to reproduce flight stresses at a selected wing station (station 214). The centers of the concentrated masses were located at station 414 on both the left and right wing outer panels. The engines and landing gear were removed, and the structure incorporating the wing and fuselage inverted and mounted between structural steel backstops as shown in figure 1. The mounting to the backstops, as shown in this figure, consisted of fabricated angles and doubler plates which distributed the stresses around the fuselage structure in a pattern similar to that which could be expected in flight.

Fatigue machine.- The constant-level fatigue machine also shown in figure 1 consisted of a prime mover, reduction gear box, line shafting, adjustable eccentric, and an exciter spring. The prime mover was a direct-current traction-type electric motor, which, along with the reduction gear box, was located as close to the center of the test setup as possible. From either side of the reduction gear box, line shafting transmitted the applied motor torque to the point of load application (station 414). The adjustable eccentric was used to convert the rotating torque to a vertical force which was transmitted to the wing through a push rod and an exciter spring. The spring was required to allow the necessary phase shift between the wing and the forcing function so that the resonance characteristics of the wing could be utilized. A detailed view of the adjustable eccentric, push rod, and exciter spring may be seen in figure 2.

The relieving load column and spring system used to simulate nacelle inertia effects may be seen in figure 1. Since the wing specimen was tested in the inverted attitude, it was necessary to install a spring system which would act opposite in direction to the motion of the wing. The back-to-back channels on the floor as well as the vertical column and engine mount made up that spring system.

INSTRUMENTATION

Each wing was instrumented with wire resistance strain gages at the nominal locations shown in figure 3. The one-active-arm strain-gage bridges shown by the squares in this figure were located so as to measure the nominal average stress in the material at points of fatigue-crack origin. The four-active-arm strain-gage bridges shown by the diamonds in the figure were located at station 220. These gages were used to measure bending moments and thus gave an indication of the constancy of the loading cycle. Recording oscillographs and the necessary balance equipment were used to record the response of the strain gages during the tests.

Each wing was also instrumented with fatigue-detector wires at locations where previous tests, in which a brittle-lacquer technique was used, had indicated points of local high stress concentrations. The nominal locations of these wires are shown by the straight and wavy dashed lines in figure 3. The fatigue-detector wires were of 0.002-inch-diameter insulated copper and were cemented to the structure in such a way that the wire would break if a fatigue crack passed under it. The breakage of the wire would be indicated at the control panel by small lights and warning bells.

A system of mechanically operated microswitches, which may be seen in figure 2, was used to count the number of times the amplitude of the wing exceeded a series of predetermined values of deflection. For operational purposes, the deflection amplitude was calibrated in terms of applied load factor.

The frequency at which the wing vibrated was held constant by an electronic speed-control unit and was indicated on a stroboscopic tachometer.

TESTS AND PROCEDURE

The method of testing chosen for the present fatigue tests on full-scale airplanes was the resonant-frequency method, in which concentrated masses were used to reproduce flight stresses at some spanwise station. It was, therefore, necessary to select the station most likely to be critical in fatigue. Examination of the wing structural analysis (reference 1) indicated that the minimum bending margins of safety existed in that region of the wing which included station 214. A distributed-load static test utilizing brittle lacquer was made for a positive low angle-of-attack condition and the results confirmed this analysis and indicated numerous spots of local high stresses at station 214. In addition, the construction at this station appeared to be reasonably representative of that used in conventional designs. For these reasons, this station was designated as critical for the present tests. The concentrated masses were located and porportioned, therefore, so as to produce the same bending moment, shear, and torque at station 214 as would be associated with air loads in level flight at positive low angle of attack. A comparison of the design bending moment, as found in reference 2, with the test applied bending moment is shown in figure 4. It may be seen that the concentrated masses reproduced the design bending moments over the inner 300 inches of the semispan. Introducing the nacelle relieving load lowered the bending moments over the inboard 175 inches and reached a maximum reduction of about 10 percent at the center line. The effect of this reduction on possible fatigue failures inboard of station 200 is somewhat indeterminate, however, because although it reduced the general stress level at a given spanwise station, it may have caused higher local stresses near the wing-nacelle juncture.

The wings were vibrated at a constant amplitude of vibration by means of the exciter spring and adjustable eccentric previously mentioned. The amplitude of vibration was equivalent to a load factor at the critical station of $1 \pm 0.625g$.

The wings were inspected during the tests to locate fatigue cracks which occurred at points other than those instrumented. This inspection was made while the wing was vibrating in an effort to keep the amplitude of vibration as nearly constant as possible by reducing to a minimum the number of times the fatigue machine was started or stopped. At various times throughout the tests, dynamic stress indications from the strain gages were recorded and checked for constancy of loading.

When a fatigue crack occurred, the number of cycles required to cause the failure was noted. The decision was then made either to stop the test, repair the crack, and thus gain more test data or to continue the test and observe the growth of the crack. The course chosen was based on the amount of data accumulated from each test specimen and the desire to observe the growth of only those cracks which seemed to be typical, rather than cracks which might be associated with details of design. Thus far the growth of only those cracks which occurred near station 214 has been observed and recorded. The cracks at this station were allowed to grow until danger to the apparatus was imminent.

RESULTS AND DISCUSSION

For the purposes of this paper, a fatigue crack is defined as one that is approximately an inch long and as deep as the material in which it started. Although all of the cracks were not discovered before they had exceeded one inch in length, the number of cycles required to cause failure was corrected to this common basis by utilizing data from other cracks on which the rate of growth had been observed as well as by utilizing indications from changes in the natural frequency of the test wings.

A summary of the loads required to cause each of the 11 fatigue cracks from the first two specimens is presented in table 2. These data are compiled in the form of the summation of cycles of load equal to or greater than the Δn values listed in the left-hand column, where Δn is the incremental load factor. The number of cycles shown in parentheses designates the number of loads applied in each class interval, that is, between consecutive values of Δn, and these loads are assumed to act at the midpoint of the class interval. For instance, for crack 1, 14,452 loads (295,085 - 280,633) are assumed to act at a Δn of 0.225 which is the mean of $\Delta n = 0.15$ and $\Delta n = 0.30$. This assumption appears reasonable in view of the fact that the load-factor increment, $\Delta n = 0.15$, is quite small, being approximately 3 percent of design ultimate load factor. Thus, the maximum error introduced should be no larger than approximately ± 1.5 percent.

As a matter of interest, the Δn values of the present data have been converted to effective gust velocities as defined in reference 3 and for the assumed operating conditions listed in table 1. These effective gust velocities are listed in the second column of table 2 and apply to a probable operating equivalent airspeed of 190 miles per hour.

Although the tests reported herein were intended to be of constant-level type at a load-factor increment of 1 ± 0.625, a number of cycles at other than this level were obtained. In general these cycles were either imposed during preliminary surveys or occurred inadvertently while the fatigue machine was being brought up to speed. The 14 cycles listed in table 2 for the first specimen at Δn values around 1.0 were imposed during static calibration tests.

In order to indicate the significance of these departures from the constant level, the number of cycles required to cause failure (for each of the 11 cracks) is shown in figure 5 in the form of frequency-distribution curves. Although only seven curves appear in figure 5, these curves represent eleven cracks since several of the cracks have identical applied loads. In this figure the number of cycles of load applied in each class interval and assumed to act at the midpoint of the interval (the numbers in parentheses in table 2) has been plotted as a function of increment of load factor Δn above the 1 g mean condition. The fact that the frequency-distribution curves are quite steep indicates that the tests were essentially of the constant-level type. It will be noted that the cycles of load applied in the class interval between a $\Delta n = 0.60$ and $\Delta n = 0.75$ were assumed to act at (and therefore were plotted at) a $\Delta n = 0.625$ rather than at the midpoint of that interval. This assumption appears reasonable in view of the relatively small number of times the applied loads were greater than the load factor value of 0.75, as well as the fact than an effort was made to keep the applied increment of load at a constant level of $\Delta n = 0.625$.

Probably the most significant point shown in figure 5, however, is the surprisingly small amount of spread in the fatigue life for each of the 11 cracks, even though all cracks did not originate at the same point in the structures. It will be noted that at $\Delta n = 0.625$, the width of the band encompassing all cracks varies from about 170,000 cycles to about 310,000 cycles. This result indicates a spread in fatigue life of a factor less than 2.

Description of fatigue cracks.- Figure 3 shows the location of the fatigue cracks on a plan view of the wing. The cracks are numbered in order of occurrence for purposes of identification. Cracks 1 to 5 were on the first specimen whereas cracks 6 to 11 were on the second specimen. In three instances involving seven of the 11 cracks, duplicate failures were obtained. Cracks 1, 2, and 11 occurred in riveted lap joints similarly located and constructed. Details of these joints are shown

in figure 6. Figures 7, 8, and 9 are photographs of the cracks. Figure 7 shows four views of crack 1 after about 50 percent of the tension material had failed. Figure 8 shows crack 2 after about 10 percent of the tension material had failed. Figure 9 shows the length of crack 11 at the time of discovery. All three of these cracks originated at the same chordwise location in the riveted joints, two on the left side of the center line of the wing, the other on the right side.

Cracks 3, 5, 8, and 9 occurred at the corners of reinforced inspection cut-outs. Figure 10 shows four views of typical cracks which started at these cut-outs and then continued to grow across the test specimen. It is interesting to note that although the crack of figure 10(a) followed a line of rivets as it propagated, the cracks in figures 10(b) and 10(c) did not.

Cracks 4 and 10 occurred in the joggle of a reinforcement doubler plate while cracks 6 and 7 occurred at the outboard juncture of the wing and engine nacelles. Figure 11 shows a typical crack in the joggle of a doubler plate and figure 12 shows the similarity of the cracks which occurred at the juncture of wing and nacelle on both left and right semispans. It should be noted that cracks 6 and 7 started in half round notches in the doubler plate. These notches had apparently been cut to provide clearance for operation of the landing gear, and their addition placed a rivet very close to the edge of the sheet.

Stress distribution.- In order to obtain an idea of the stress distribution in the region of the fatigue cracks, the second specimen was instrumented with strain gages which were located in regions where cracks were obtained in the first specimen. (See fig. 3.)

The strain gages were located so as to measure only the nominal average stress in the material in the vicinity of the points where the fatigue cracks originated. In fact the gages were placed far enough away from the point of fatigue crack origin so as to exclude the effect of stress concentrations. A typical installation of these strain gages can be seen in figure 9. An example of the chordwise stress distribution as measured in the vicinity of the riveted joints where cracks 1, 2, and 11 originated is shown in figure 13. In this figure maximum measured stress - that is, the alternating stress plus the mean stress - is plotted as a function of strain-gage location in inches forward of the 70-percent-chord position. It is interesting to note that the fatigue cracks originated at the same approximate distance from the 70-percent-chord position as the point of maximum measured stress shown in figure 13.

Effective stress-concentration factor.- Since stress concentrations were not measured directly, an effective stress-concentration factor was deduced from the data by several methods. For a constant-level test, this factor could easily be obtained by dividing the stress required to cause failure (as found from standard S-N curves of unnotched alclad material) by the measured stress. In order to pursue this method of analysis for the present calculations, the assumption was made that only those cycles of load which had been applied between $\Delta n = 0.60$ and $\Delta n = 0.75$ caused any fatigue damage. It was further assumed that those loads acted at a value of $\Delta n = 0.625$ instead of the midpoint of the class interval. This assumption appears reasonable inasmuch as an effort was made to maintain a constant load-factor increment of $1 \pm 0.625g$.

The results of these calculations for cracks where stress measurements were available are as shown in table 3. Columns 1 and 2 of this table enumerate the fatigue cracks and give a short description of the point where the cracks originated. Column 3 gives the number of cycles to failure at a value of Δn of 0.625. Columns 4 and 5 give the measured mean stress σ_{mean} and the measured maximum stress σ_{max} for the four failures where measured stresses were available. Column 6 gives the stress σ_{SN} which would cause failure at the number of cycles listed in column 3. The effective stress-concentration factor K_1 is given in column 7 and is defined as:

$$K_1 = \frac{\sigma_{SN}}{\sigma_{max}}$$

In this expression σ_{SN} is that value obtained from the S-N curve for which a mean stress equal to σ_{mean} times K_1 applies. The quantities K_1 and σ_{SN} are interdependent; that is, K_1 is used to determine σ_{SN} and σ_{SN} in turn is used to define K_1. In order to determine the value of K_1 for each failure, a trial-and-error method is employed wherein different values are assigned to K_1 until one value is found which satisfies both conditions. The S-N curves used to determine σ_{SN} were based on data for 0.040-inch-thick unnotched alclad 24S-T sheet as given in reference 4. The factor K_1 for the constant-level analysis varied from 2.58 to 3.15 for identical riveted joints; whereas the one value computed for the corner of an inspection cut-out was 4.20.

Since the amplitude of the applied stress cycles was not exactly at a constant level during the present tests, the cumulative-damage theory described in reference 5 was also used to compute an effective stress-concentration factor, K_2. This theory basically states that failure will occur when the summation curve of the loading cycles becomes tangent to the S-N curve. The determination of K_2 by this theory is illustrated in figure 14 for one of the four fatigue cracks at which stress measurements were available. Data on unnotched 0.040 24S-T Alclad sheet reported in reference 4 were also used to plot the S-N curves shown in this figure. The solid lines in figure 14 show the S-N curves for the pertinent mean stress values. The dashed lines represent the summation curves, or the number of loads applied equal to or greater than the listed stress values. The lower dashed line represents measured stress values whereas the upper dashed line represents the measured stress values moved vertically until they became tangent to the S-N curve having the proper mean stress value. This adjustment, in effect, was accomplished by multiplying the measured stress values by a constant, which is the effective stress-concentration factor K_2 listed in column 9 of table 3. The fact that the values of K_1 and K_2 agree so closely indicates that the tests were essentially of the constant-level type. This can readily be seen since those loads applied at other than $\Delta n = 0.625$ apparently had a negligible effect upon the effective stress-concentration factor.

The Miner theory of reference 6 was also used to check the results of the present tests. Miner's theory basically assumes that fatigue failure will occur when $\sum \frac{p}{N} = 1$, where

p number of cycles of load applied at each value of Δn, or stress level

N number of cycles of load required to cause failure at the pertinent stress levels as found from S-N curves

The results of these calculations are also tabulated in table 3 under column 12 and vary from 1.04 to 1.21. It should be pointed out here that these calculations do not necessarily prove the Miner theory to be either true or false but show only a measure of the variation of the present tests from the true constant-level type.

Rate of growth.- Cracks 3 and 4, which originated near station 214, were detected by fatigue-detector wires at an early stage and were allowed to grow until danger to the equipment was imminent. The rate at which the cracks grew is shown in figure 15 where the estimated loss of total tension material, in percent of cross-sectional area of the tension surface at this station, is shown as a function of cycles of applied load. It is interesting to note that the growth of the cracks

was relatively slow until about 7.5 percent of the tension material had failed. The slopes of the curves then become very steep, indicating a very rapid propagation of the crack.

Effect on frequency and damping.- The present tests indicated that the natural frequency of the wing was not affected by fatigue damage until after a fatigue crack had originated. Even then, the frequency decreased only by about 2 cycles per minute (out of 106 cpm) when as much as 55 percent of the tension material had failed. Figure 16 shows the indicated reduction in natural frequency plotted as a function of percentage loss of tension material for cracks 3 and 4. Although there is some scatter in data, the two curves apparently have the same general shape.

No specific damping measurements were made during the present tests, but the indications were that the damping did not change as the fatigue life was used up. This statement is based primarily on the fact that the amplitude of vibration, for a set operating condition, did not change until after a fatigue crack had originated. The damping of these wings was quite low (reference 7), and the relative magnification curve was therefore very steep. Also, since the tests were conducted at resonant frequency, any change in damping would have caused a very pronounced change in amplitude of vibration but no such change was noted.

Inasmuch as neither the natural frequency nor the damping of the two test wings appeared to be affected by fatigue damage until after a fatigue crack had originated, the use of these parameters does not appear adequate as a measure of the damage caused by fatigue in an airplane wing structure.

CONCLUDING REMARKS

Although the results cover 11 fatigue cracks, sufficient data are not yet available to permit the formulation of definite conclusions. The data do indicate a surprisingly small amount of spread in fatigue life even though all fatigue cracks did not originate at the same points.

Although the tests reported herein were not of an exact constant-level type according to standards set forth in fatigue tests of small specimens, calculations indicated that essentially all the fatigue damage was done at the desired level of stress amplitude. Computed effective stress-concentration factors for the riveted joints varied from 2.55 to 3.15. The one value computed for the corner of one inspection hole cut out was 4.20. Neither the natural frequency nor the damping

of the two test specimens appeared to be affected by fatigue damage until after a fatigue crack had originated; the use of these parameters therefore may not be adequate as a measure of fatigue damage. The rate of fatigue-crack growth was quite small until approximately 7.5 percent of tension material failed, after which the rate of crack growth increased markedly.

Langley Aeronautical Laboratory
National Advisory Committee for Aeronautics
Langley Field, Va.

REFERENCES

1. Nilsen, R. T., and Bradley, R. T.: Wing Analysis (Section Properties and Stresses) Model 20-B (C-46). Vol. I. Rep. No. 20-C10, Curtiss-Wright Corp., Airplane Div. (St. Louis), March 10, 1942.

2. Anon.: General Analysis - Calculation of Applied External Wing Loads. Model 20-B (C-46), Rep. No. 20-A4, Curtiss-Wright Corp., Airplane Div. (St. Louis), March 6, 1942.

3. Donely, Philip: Summary of Information Relating to Gust Loads on Airplanes. NACA Rep. 997, 1950. (Formerly NACA TN 1976.)

4. Russell, H. W., Jackson, L. R., Grover, H. J., and Beaver, W. W.: Fatigue Strength and Related Characteristics of Aircraft Joints. II - Fatigue Characteristics of Sheet and Riveted Joints of 0.040-Inch 24S-T, 75S-T, and R303-T275 Aluminum Alloys. NACA TN 1485, 1948.

5. Bland, Reginald B., and Sandorff, Paul E.: The Control of Life Expectancy in Airplane Structures. Aero. Eng. Rev., vol. 2, no. 8, Aug. 1943.

6. Miner, Milton A.: Cumulative Damage in Fatigue. Jour. Appl. Mech., vol. 12, no. 3, Sept. 1945.

7. Fearnow, Dwight O.: Investigation of the Structural Damping of a Full-Scale Airplane Wing. NACA RM L51A04, 1951.

TABLE 1

GEOMETRIC CHARACTERISTICS OF C-46D AIRPLANE PERTINENT TO FATIGUE PROGRAM

Normal gross weight, pounds	45,000
Assumed operating weight, pounds	40,000
Minimum flying weight, pounds	26,195
Level flight equivalent airspeed, miles per hour	240
Probable operating equivalent airspeed, miles per hour	190
Design gliding equivalent airspeed, miles per hour	310
Airfoil section from center line to station 192	NACA 23017
Airfoil section from station 192 to tip changes gradually to	NACA 4401.5
Wing area, square feet	1360
Wing span, feet	108
Tip chord, theoretical, inches	66
Root chord, inches	198
Taper ratio	0.333
Mean aerodynamic chord, inches	164.25
Incidence at wing root, degrees	3.5
Incidence at wing tip, degrees	0.5
Dihedral at 70 percent chord, degrees	7.0
Angle between 70 percent chord and center line, degrees	90
Sweepback, leading edge, degrees	11.4
Aspect ratio	8.58

TABLE 2

LOAD HISTORY FOR EACH OF ELEVEN CRACKS

Δn	Effective gust velocity U_e (ft/sec)	Summation of applied loads equal to or greater than Δn threshold value[1]										
		Crack 1 (cycles)	Crack 2 (cycles)	Crack 3 (cycles)	Crack 4 (cycles)	Crack 5 (cycles)	Crack 6 (cycles)	Crack 7 (cycles)	Crack 8 (cycles)	Crack 9 (cycles)	Crack 10 (cycles)	Crack 11 (cycles)
0.15	2.5	295,085	332,048	332,048	353,999	446,815	222,861	222,861	222,861	222,861	332,022	369,914
0.225		(14,452)	(17,068)	(17,068)	(18,270)	(19,193)	(4,019)	(4,019)	(4,019)	(4,019)	(6,660)	(7,324)
0.30	4.9	280,633	314,980	314,980	335,729	427,676	218,842	218,842	218,842	218,842	325,362	362,590
0.375		(29,794)	(31,727)	(31,727)	(34,950)	(36,885)	(10,889)	(10,889)	(10,889)	(10,889)	(11,785)	(12,610)
0.45	7.4	250,839	283,253	283,253	300,779	390,791	207,953	207,953	207,953	207,953	313,577	349,980
0.525		(71,842)	(80,620)	(80,620)	(89,232)	(98,928)	(28,997)	(28,997)	(28,997)	(28,997)	(31,344)	(33,837)
0.60	9.9	178,997	202,633	202,633	211,547	291,863	178,956	178,956	178,956	178,956	282,233	316,143
0.675		(170,340)	(193,976)	(193,976)	(202,890)	(280,299)	(170,547)	(170,547)	(170,547)	(170,547)	(273,645)	(307,555)
0.75	12.4	8,657	8,657	8,657	8,657	11,564	8,409	8,409	8,409	8,409	8,588	8,588
0.825		(8,507)	(8,507)	(8,507)	(8,507)	(11,414)	(8,409)	(8,409)	(8,409)	(8,409)	(8,588)	(8,588)
0.90	14.9	150	150	150	150	150	0	0	0	0	0	0
0.975		(136)	(136)	(136)	(136)	(136)	0	0	0	0	0	0
1.05	17.3	14	14	14	14	14	0	0	0	0	0	0
1.125		(14)	(14)	(14)	(14)	(14)	0	0	0	0	0	0

[1]The number of cycles shown in parenthesis designates the loads applied in each class interval and assumed to act at the midpoint.

TABLE 3

SUMMARY OF ACCUMULATED DATA

(1) Fatigue crack	(2) Fatigue-crack location[1]	(3) Applied loads at $\Delta n = 0.625$ (cycles)	(4) Measured Stress σ_{mean} (psi)	(5) Measured Stress σ_{max} (psi)	(6) Stress found from S-N curve σ_{SN} (psi)	(7) Effective stress concentration factor K_1	(8) Summation of applied loads $\geq \Delta n = 0.60$ (cycles)	(9) Effective stress concentration factor K_2	(10) Effective mean stress, $K_2\sigma_{mean}$	(11) Effective maximum stress, $K_2\sigma_{max}$	(12) $\sum \frac{p}{N}$
1	Riveted joint (L, CS)	170,340	7,978	13,053	41,133	3.15	178,997	3.10	24,732	40,464	1.21
2	Riveted joint (R, CS)	193,976	9,659	15,591	40,225	2.58	202,633	2.55	24,630	39,757	1.16
3	Inspection cut-out (R, OP)	193,976	5,506	9,223	38,737	4.20	202,633	4.15	22,850	38,275	1.18
4	Joggle in doubler plate (L, OP)	202,890	-----	------	------	----	211,547	----	------	------	----
5	Inspection cut-out (L, OP)	280,299	-----	------	------	----	291,863	----	------	------	----
6	Juncture of wing and nacelle (R, CS)	170,547	-----	------	------	----	178,956	----	------	------	----
7	Juncture of wing and nacelle (L, CS)	170,547	-----	------	------	----	178,956	----	------	------	----
8	Inspection cut-out (R, CS)	170,547	-----	------	------	----	178,956	----	------	------	----
9	Inspection cut-out (L, CS)	170,547	-----	------	------	----	178,956	----	------	------	----
10	Joggle in doubler plate (L, CS)	273,645	-----	------	------	----	282,233	----	------	------	----
11	Riveted joint (L, CS)	307,555	7,744	12,436	37,059	2.98	316,143	2.95	22,845	36,686	1.04

[1]Letters refer to following:
L - Left wing
R - Right wing
CS - Center section
OP - Outer panel

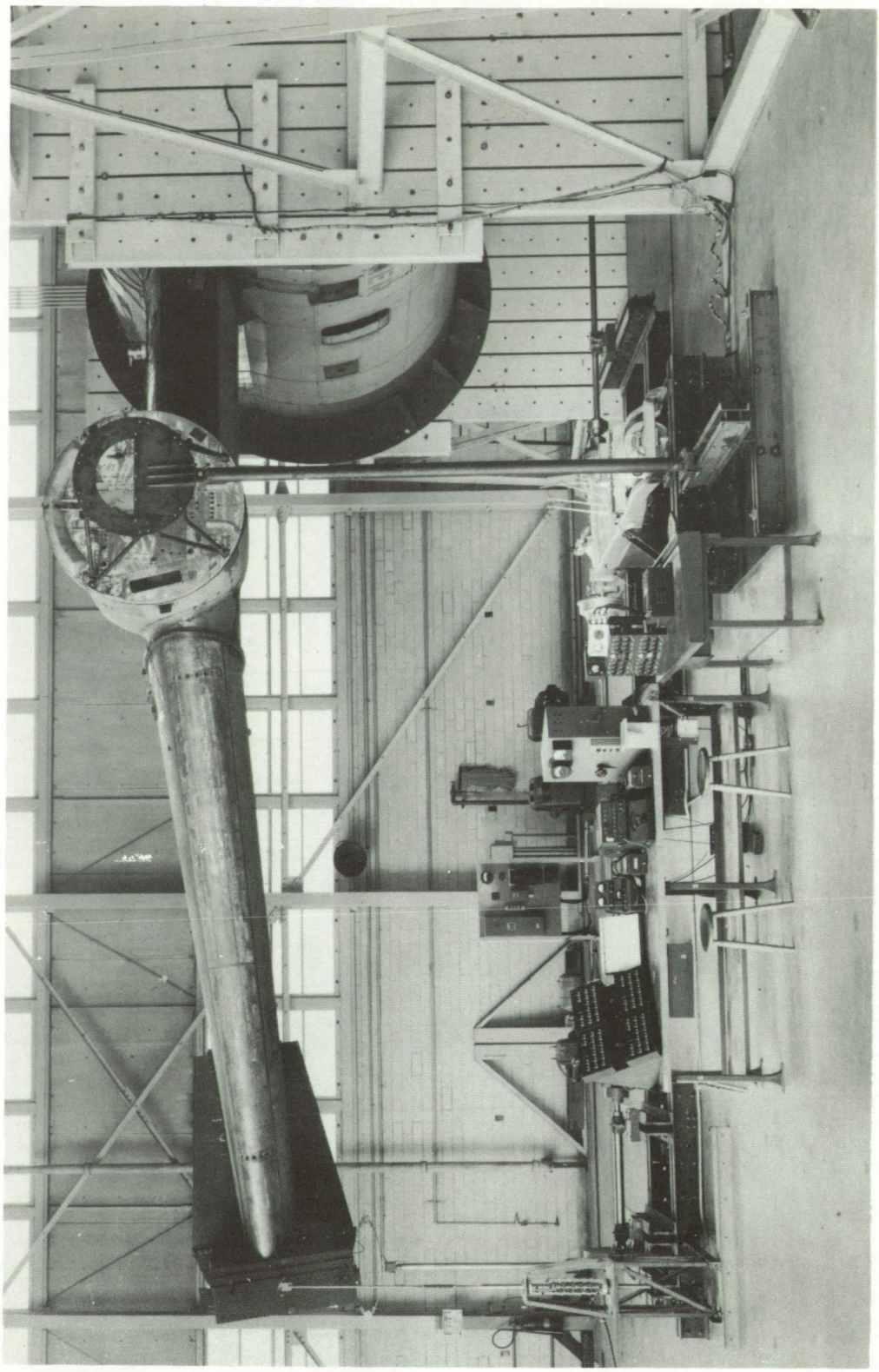

NACA L-85838

Figure 1.- General view of left half of test setup.

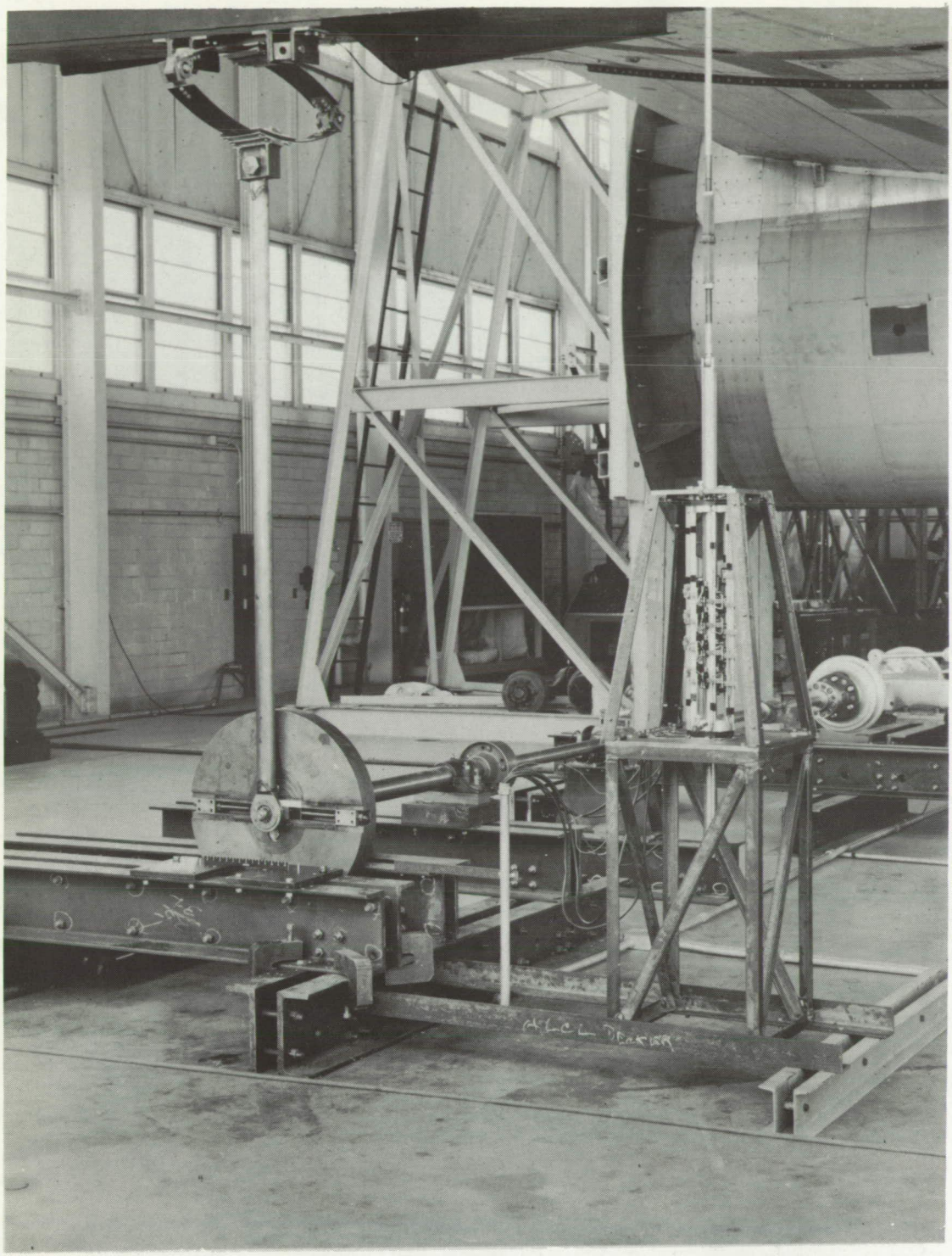

NACA

L-65841

Figure 2.- Detailed view of exciter spring system and amplitude-measuring microswitch assembly.

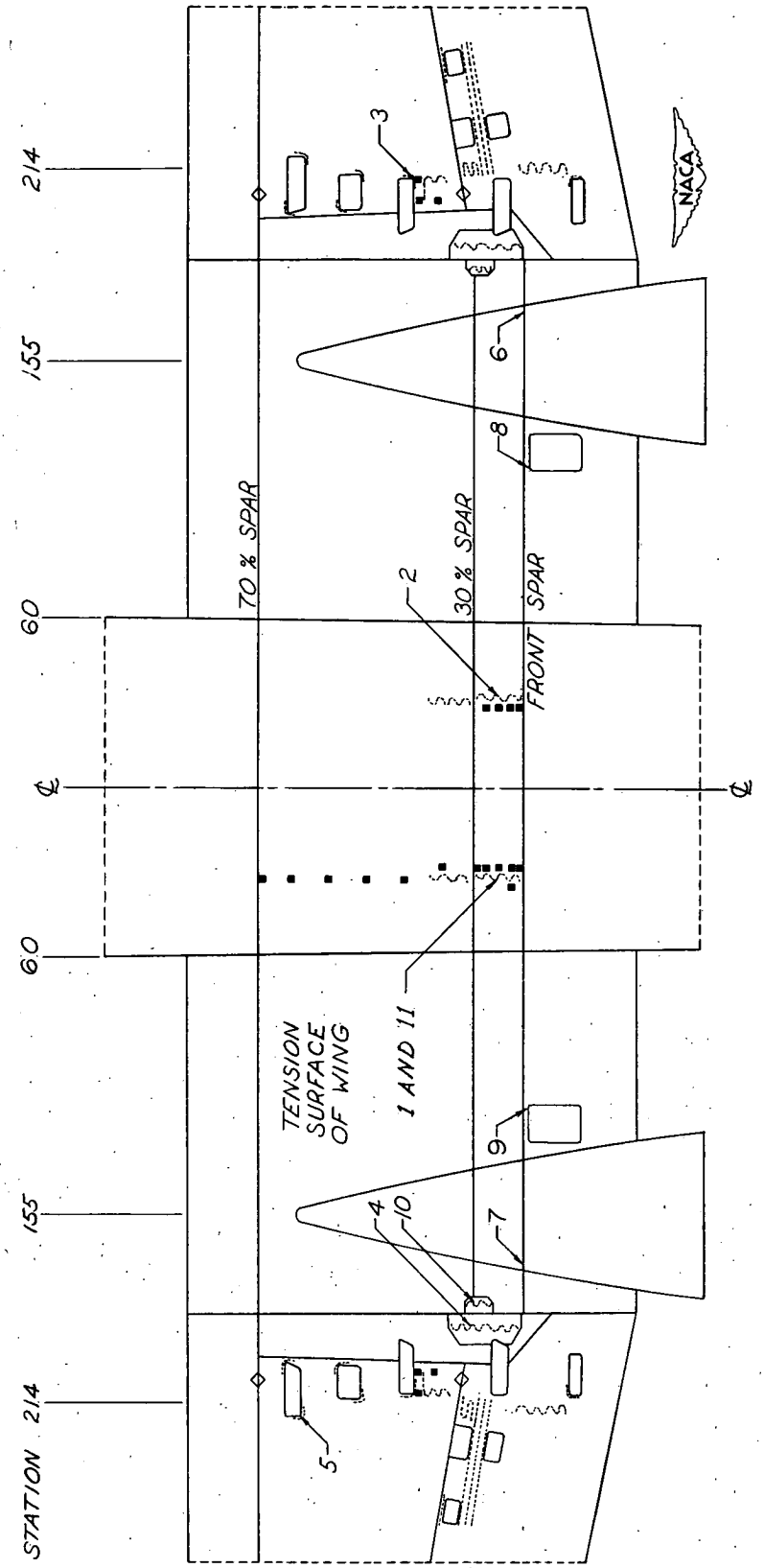

Figure 3.- Nominal location of instrumentation and point of crack origin.

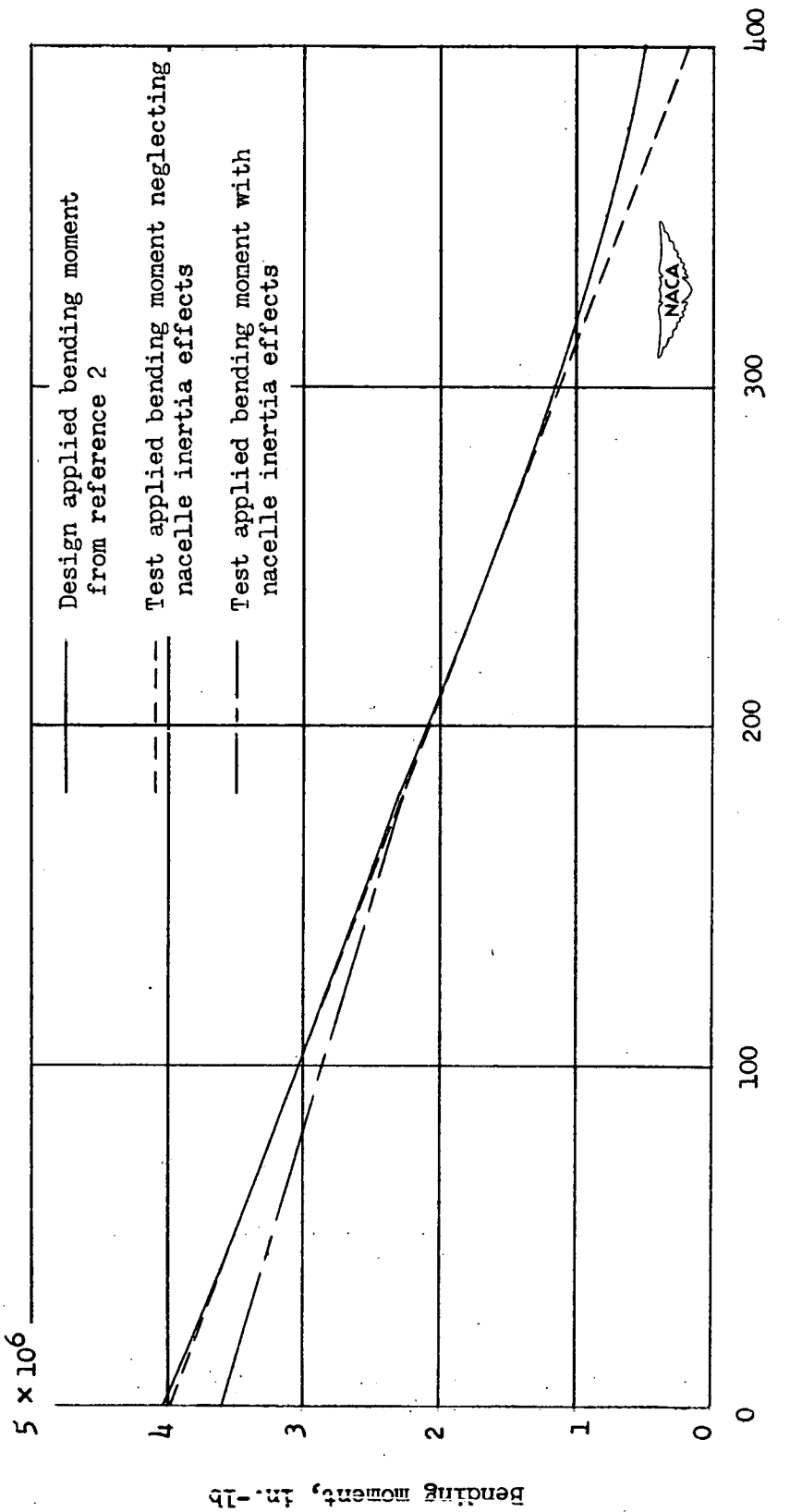

Figure 4.- Comparison of design and test applied bending moment for level-flight condition.

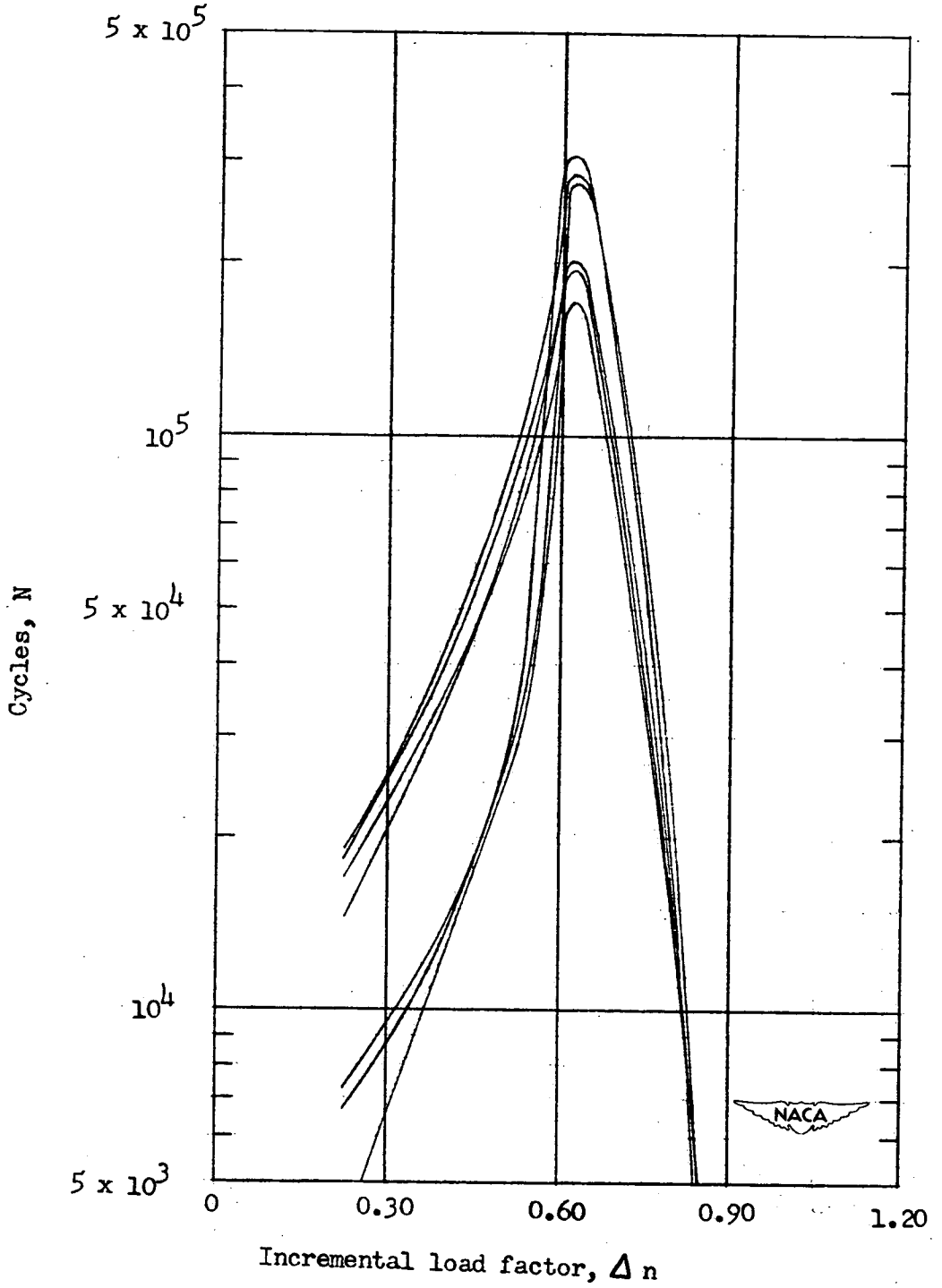

Figure 5.- Frequency distribution of applied loads.

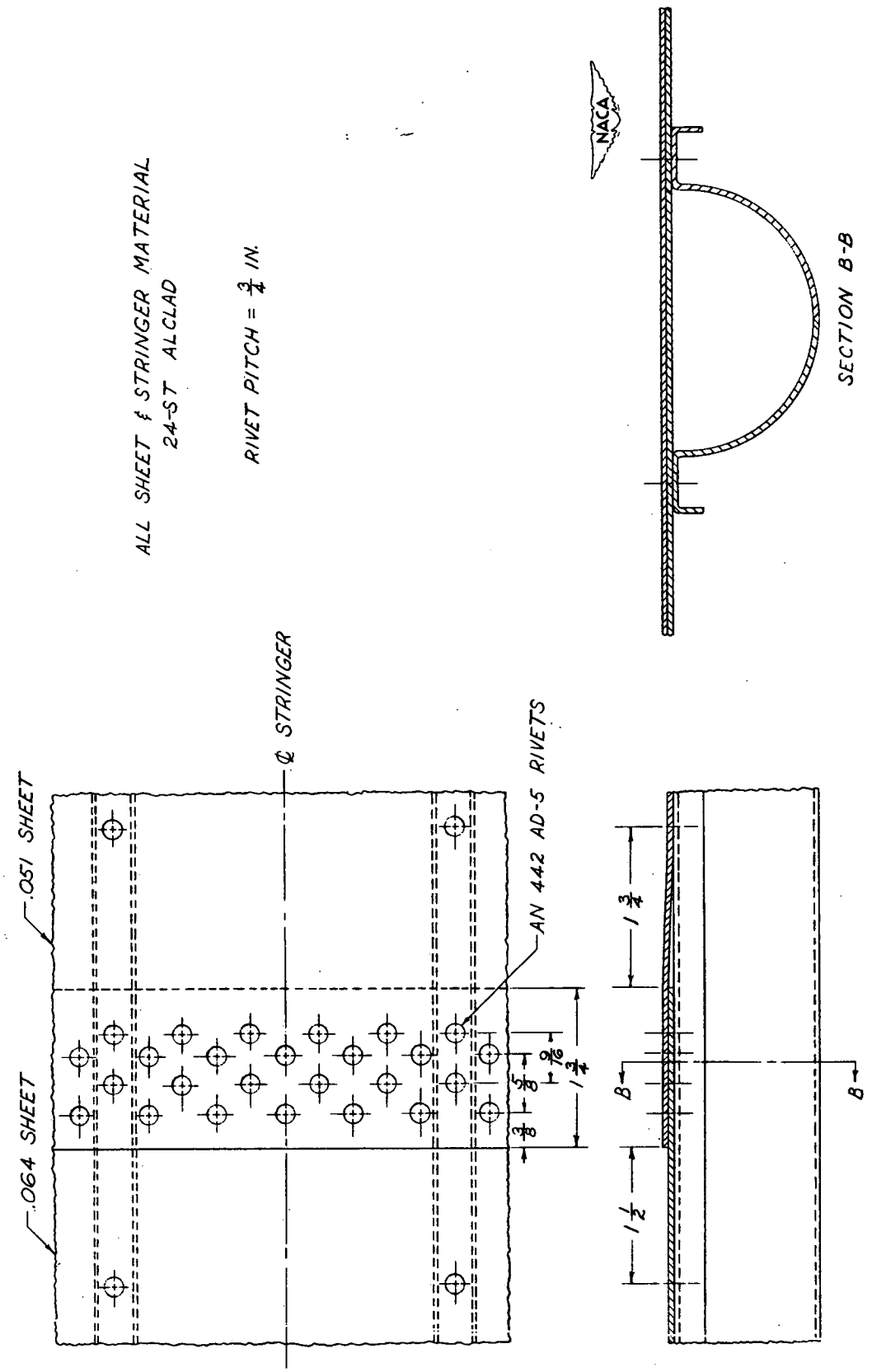

Figure 6.- Details of riveted joint where cracks 1, 2, and 11 originated.

(a) View of crack looking aft.

(b) View of crack aft of point of origin.

(c) View of crack from inside of wing.

NACA
L-68451

(d) View of crack showing failure of front spar flange.

Figure 7.- Four views of left wing showing crack 1 after loss of 50 percent of the tension material.

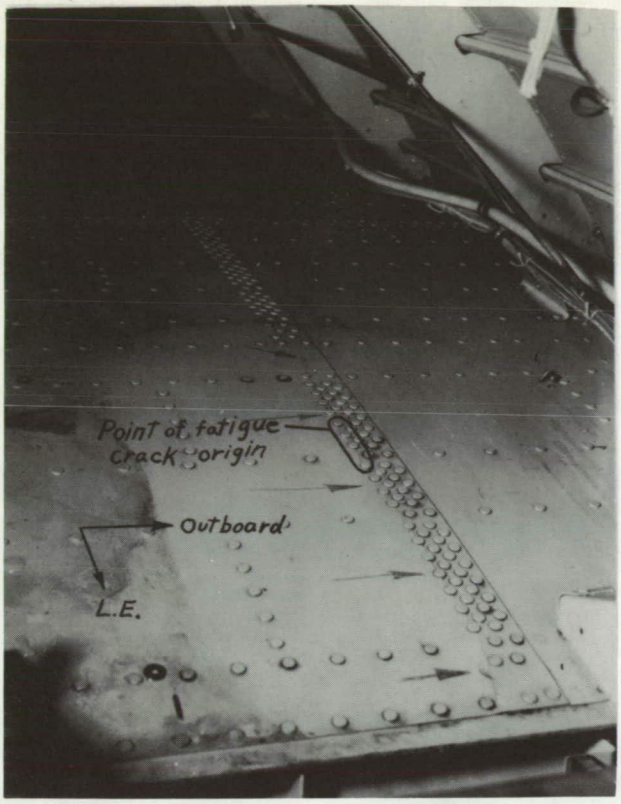

NACA
L-68452

Figure 8.- View of right wing showing crack 2.

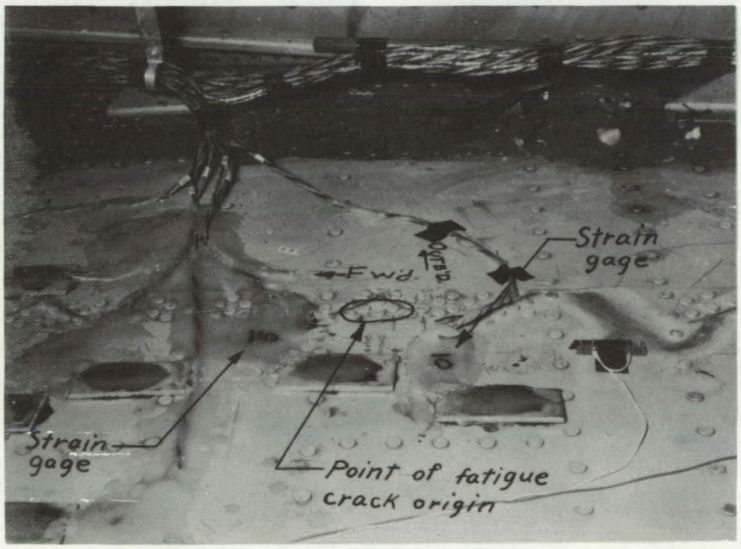

NACA
L-68453

Figure 9.- View of left wing showing crack 11 when discovered.

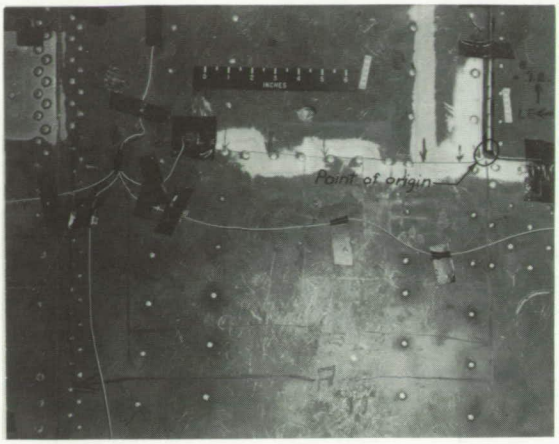

(a) View of crack 3 on right wing.

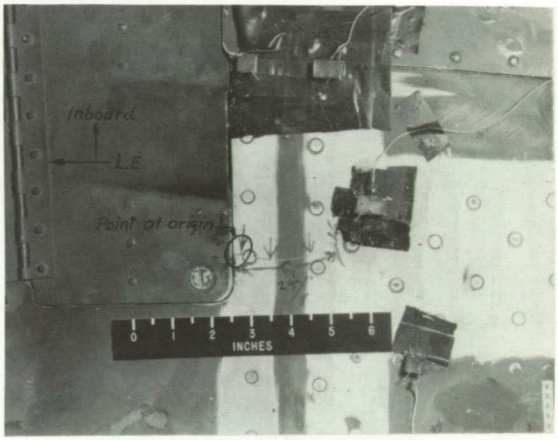

(b) View of crack which started as a secondary effect of crack 3.

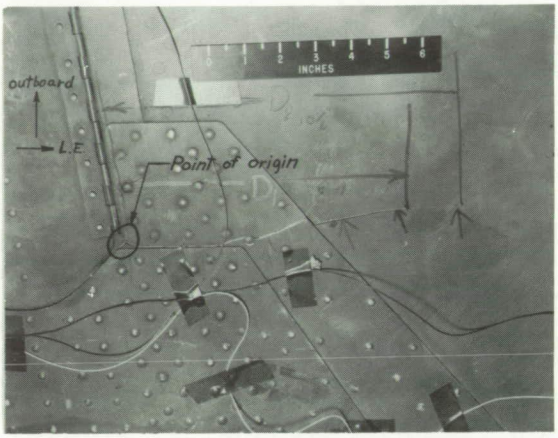

(c) View of crack which started as a secondary effect of crack 3.

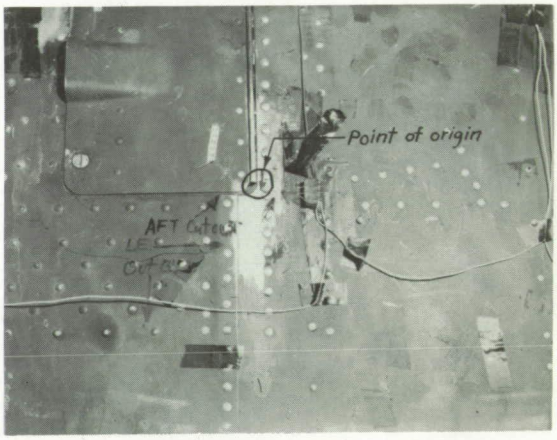

NACA
L-68454

(d) View of crack 5 on left wing.

Figure 10.- View of typical cracks originating at corners of inspection holes.

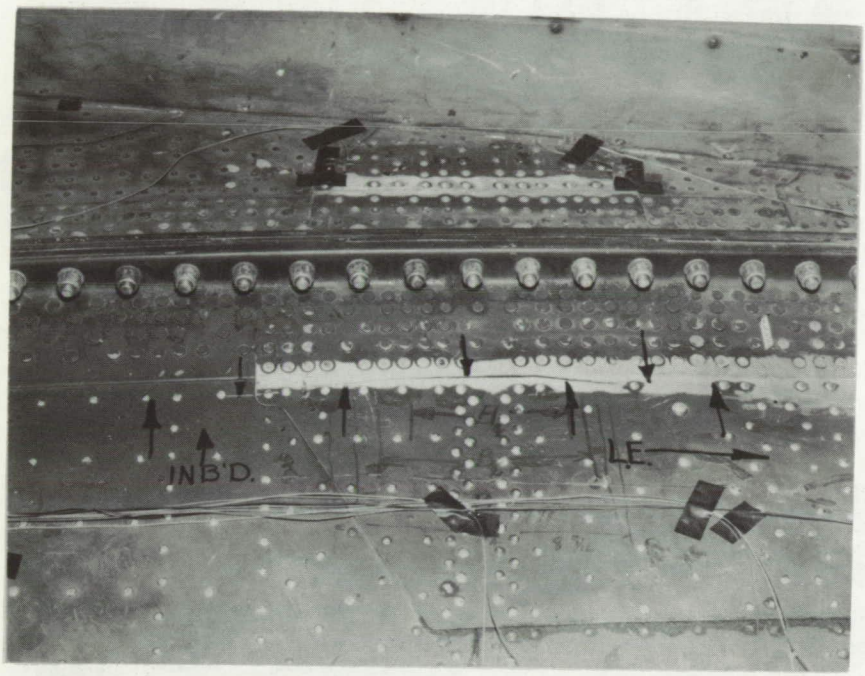

NACA

L-67351

Figure 11.- View of typical crack in doubler plate, crack 4.

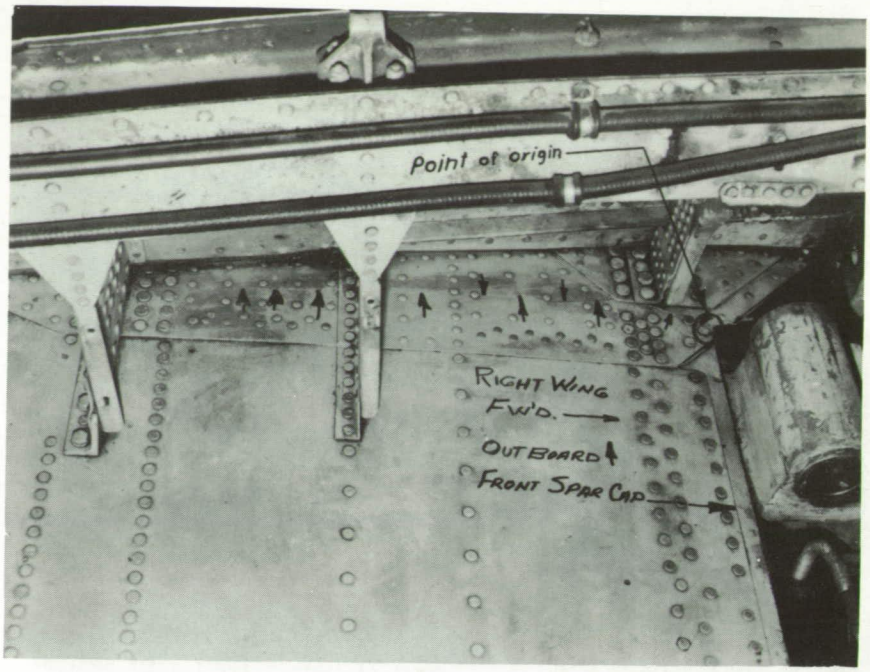

(a) View of crack 6.

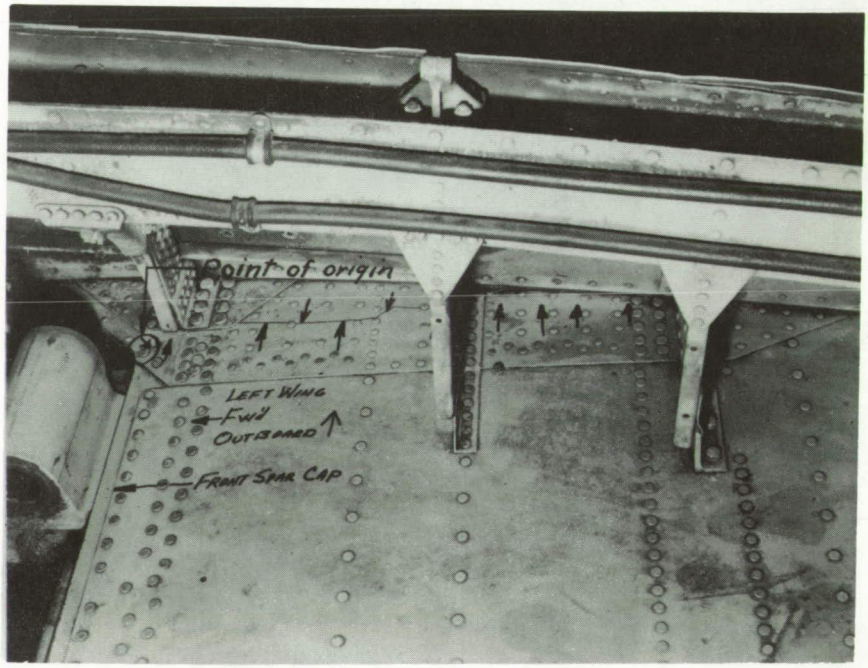

(b) View of crack 7.

NACA
L-68455

Figure 12.- Typical cracks at juncture of wing and engine nacelle.

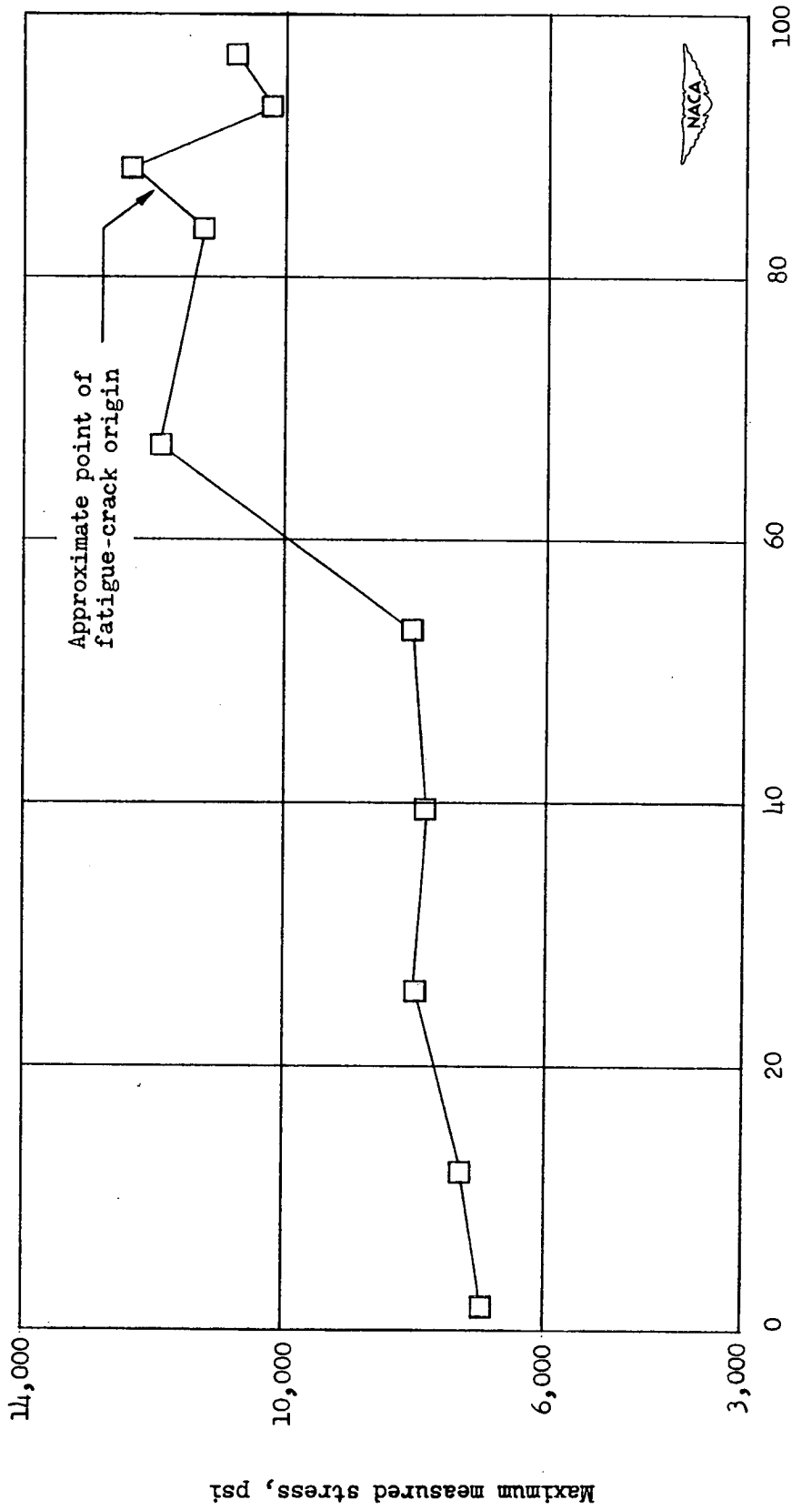

Figure 13.- Chordwise distribution of measured stress at riveted joint where cracks 1, 2, and 11 originated.

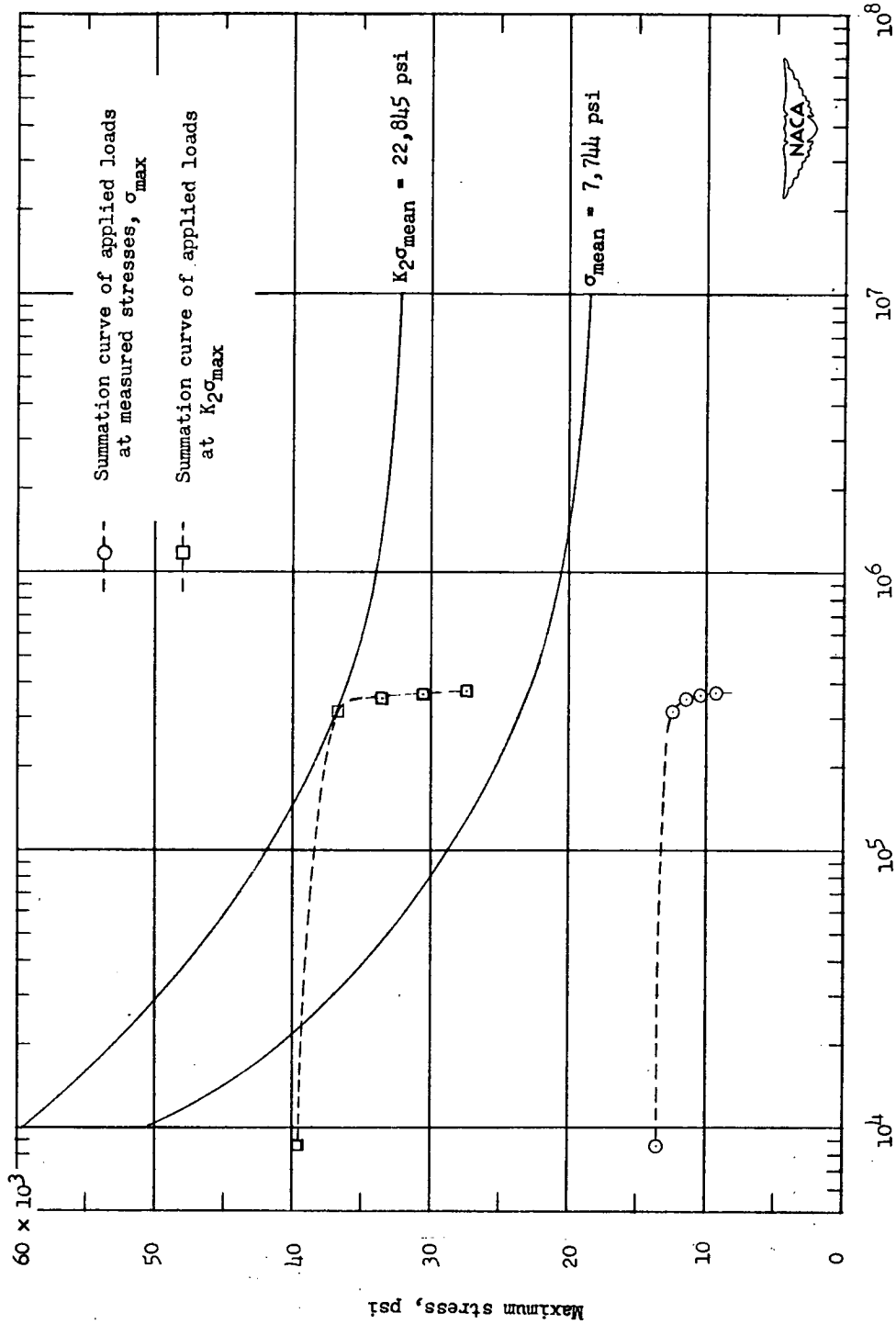

Figure 14.- Typical expansion of summation curves for determination of effective stress-concentration factor, K_2.

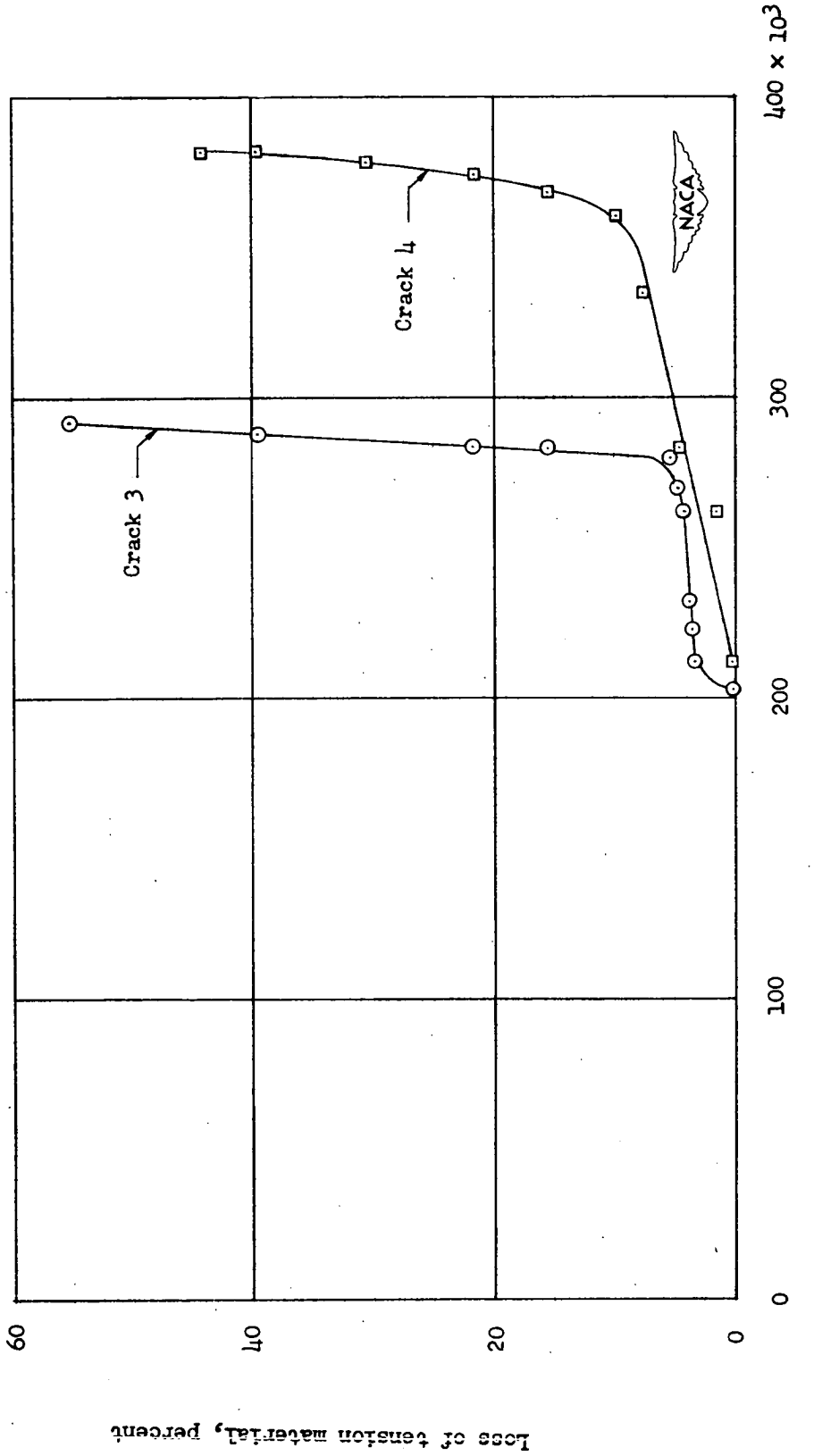

Figure 15.- Growth of fatigue cracks 3 and 4.

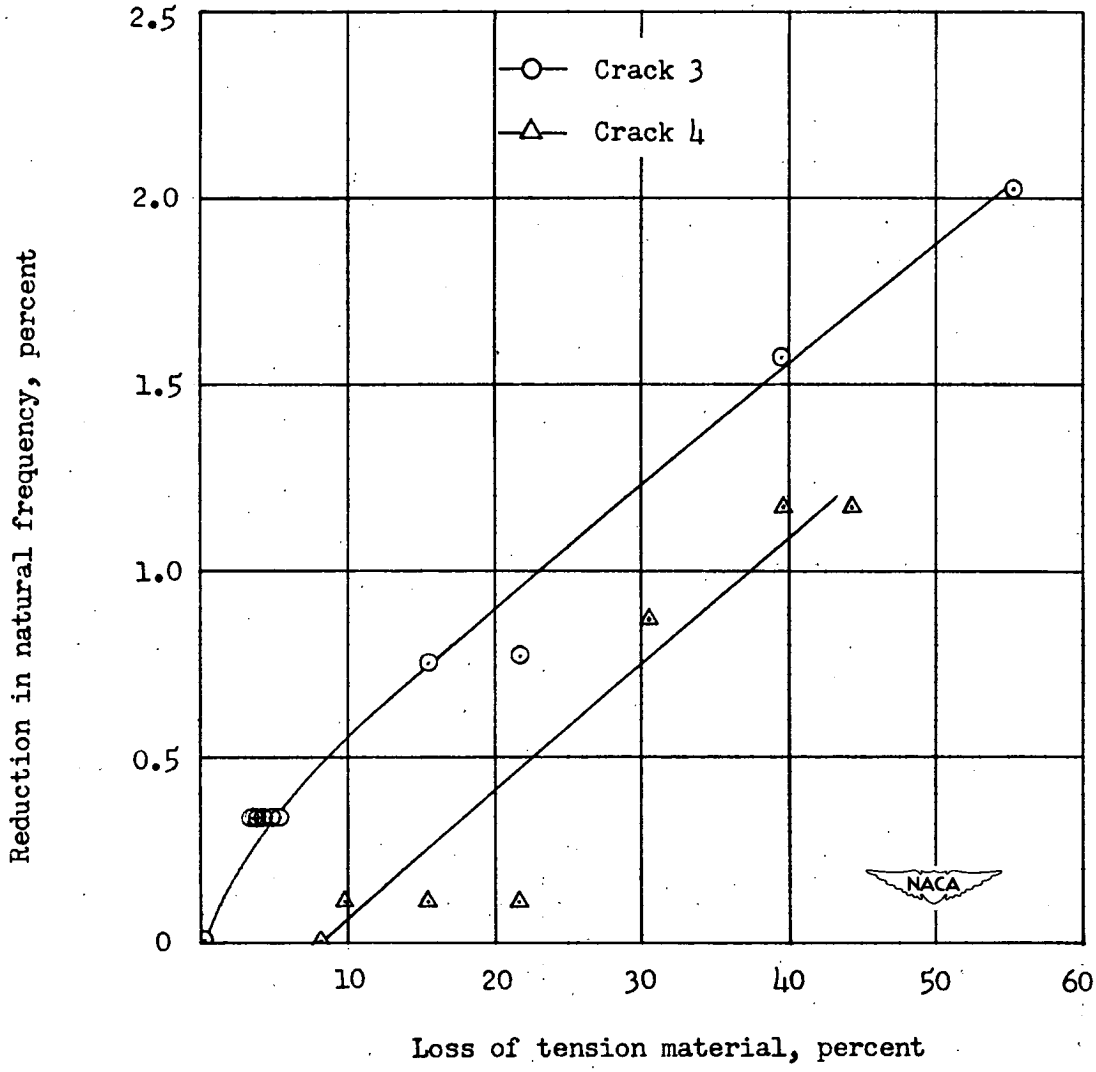

Figure 16.- Variation of natural frequency of test specimen with loss of tension material.